water

MDPI

Article

Soil Loss Estimation Coupling a Modified USLE Model with a Runoff Correction Factor Based on Rainfall and Satellite Soil Moisture Data

Francesca Todisco [1,*], Lorenzo Vergni [1], Sofia Ortenzi [2] and Lucio Di Matteo [2]

[1] Department of Agricultural, Food and Environmental Science, University of Perugia, 06124 Perugia, Italy; lorenzo.vergni@unipg.it
[2] Department of Physics and Geology, University of Perugia, 06123 Perugia, Italy; sofia.ortenzi@studenti.unipg.it (S.O.); lucio.dimatteo@unipg.it (L.D.M.)
* Correspondence: francesca.todisco@unipg.it; Tel.: +39-075-5856052

Abstract: Satellite observations (Copernicus Sentinell-1) can supply antecedent soil moisture data, which helps to predict thresholds triggering runoff and runoff volume. In the paper, we developed a runoff correction factor to the USLE, using rainfall and satellite antecedent soil moisture data, following the approach of the modified USLE models such as the USLE-M and USLE-MM. The runoff and soil loss estimations accuracy are validated by plot-scale measurements (2008–2020 period) provided by SERLAB (Soil Erosion Laboratory) of the University of Perugia. The results show that the event rainfall depth added to the antecedent soil moisture is a fairly suitable predictor of the runoff. Using the simulated runoff in a USLE-MM model, the capability to predict event soil losses is enhanced with an RMSE = 0.57 Mg/ha lower than the RMSE ≈ 3.1 Mg/ha obtained by the USLE model. Using a modified USLE model, albeit with remote estimated runoff data, is still more advantageous at the event scale than the USLE model, which does not consider the runoff. These results are particularly significant for the estimation of runoff and soil losses. Satellite data shows the potential of applying the modified USLE models for large-scale monitoring and quantification of event soil erosion and runoff.

Keywords: USLE; remote sensing; soil water erosion; Copernicus Sentinel-1; runoff thresholds; runoff generation; rainfall runoff erosivity factor; runoff models; erosion models; hydrological processes seasonality

check for updates

Citation: Todisco, F.; Vergni, L.; Ortenzi, S.; Di Matteo, L. Soil Loss Estimation Coupling a Modified USLE Model with a Runoff Correction Factor Based on Rainfall and Satellite Soil Moisture Data. *Water* **2022**, *14*, 2081. https://doi.org/10.3390/w14132081

Academic Editor: Nufang Fang

Received: 29 April 2022
Accepted: 27 June 2022
Published: 29 June 2022

1. Introduction

Several models (empirical, conceptual, physical, and process-oriented) have been proposed to estimate soil loss at different spatial and temporal scales [1,2]. The empirical approaches, among which the Universal Soil Loss Equation (USLE) and its subsequent updates (RUSLE and RUSLE2) [3] dominate, continue to find a wide application at all the spatial scales [4,5]. The reason for this diffusion of USLE models is to be found in the relative ease of application and reliability of the estimates [6]. The growing availability of remote sensing data, useful for quantifying USLE factors [7], has increased its popularity even more. On the other hand, the original USLE model [8], developed to predict the long-term average annual soil loss, cannot be considered the most effective tool for planning soil conservation measures since a large fraction of the total soil loss in a given area is due to a relatively few large storms [9,10]. The most common way to improve the reliability of the USLE model at the event scale is to modify the rainfall erosivity factor by multiplying it by the runoff coefficient (i.e., the ratio of the event runoff to the event rainfall depth) as in the USLE-M [11] and USLE-MM models [12,13]. Runoff, however, is not just a function of certain constant characteristics of the soil and the space-time characteristics of the rainfalls. On the contrary, using runoff means knowing how to predict it with reasonable precision through sufficiently accurate models, applicable in most cases. Todisco et al. [14] explained that although the modification of the erosivity with the runoff coefficient makes the USLE/RUSLE model more accurate at the event scale, it also makes its application more difficult, given the poor availability of runoff measurements. This problem can be solved by employing rainfall runoff simulation models, but in the literature, there are only a few examples of the application of USLE/RUSLE models in combination with rainfall runoff models [14–16]. The reason lies in the complexity of the rainfall runoff processes, which depend on several interacting factors, such as topographic characteristics, meteo-climatic conditions (including rainfall intensity and duration), lithological and hydraulic properties of soils, vegetation cover types, agricultural practices, etc. [17–20]. A recent approach to this problem is investigating the threshold patterns in stormflow resulting from changes in antecedent moisture conditions such as antecedent volumetric water content (θ), Antecedent Soil Moisture Index (ASI), degree of saturation (Sr), or a combination of these with cumulated rainfall, P, (e.g., ASI + P). The ASI index was introduced by [21]; it is expressed in mm, and it is defined by the product of the average volumetric water content (θ) and the depth of investigation (D). Some of these parameters are widely available all over the Earth as satellite data. Detty et al. [19] highlighted a high correlation between ASI + P and quick flow volumes for 13 runoff events, investigating runoff generation mechanisms in till-mantled headwater catchment (NH, USA). Penna et al. [22] proposed a threshold between θ and streamflow, analyzing a small alpine headwater catchment located in the Italian Dolomites. In detail, soil moisture and streamflow started to rise concurrently during wet conditions, while soil moisture peaked earlier than streamflow during dry conditions. In addition, runoff resulting from changes in antecedent moisture conditions was investigated. Ali et al. [23] reported different nonlinear input-output relationship shapes, such as the hockey stick shape [24], step function (or Heaviside) [25], Dirac function [26], and sigmoid function [27]. Threshold behavior in different ecohydrological processes (e.g., runoff generation) is strictly related to the spatial and temporal scales, climatic conditions, and physical controls. Following [23], other studies focused on the hydrologic response threshold values, trying to explain what might drive the differences among the sites. [28], noticed differences in runoff coefficients and hydrological dynamics between summer and fall/spring rainfall events, which were related to ASI + P. The study on a small, forested catchment in the Italian Pre-Alps equipped with soil moisture probes, weirs, and piezometers suggested a mix of intensity-dependent and wetness-dependent processes (ASI + P) controlling the runoff production mechanism. As reported by [29], seasonal variations in the threshold behaviors depend on vegetation canopy interception and wet/dry conditions. Scaife et al. [30] obtained different ASI + P thresholds on three forested catchments in North Carolina (USA). In these cases, maximum hourly rainfall intensity had a relatively small effect on quick flow generation compared to ASI + P. The authors presented straight lines above and below the thresholds, which are useful to compute the runoff based on ASI + P values. The role of P and ASI + P on the surface, subsurface, and epikarst seepage runoff (SR, SSR, and ESR) have been recently investigated in twelve 5 × 20 m karst plots in southwest China [31]. Based on the various shapes of the relationship between P or ASI + P and runoff [23], different models for karst slopes, such as hockey stick, step function, and the sigmoid function, have been detected [31]. Therefore, using P or ASI + P to derive generation thresholds (triggering stormflow), rise thresholds (rapid responses of stormflow), and predict runoff is challenging. The cited studies are focused on equipped small catchments or plots, where the volumetric water content is monitored continuously to capture the moisture content before the stormflow event. Unfortunately, the water content is not monitored in most of the small catchments worldwide, and when done, the data acquired may not represent the whole basin. Moreover, soil moisture equipment for continuous monitoring, especially those working at low frequency, needs to be calibrated before their use in the field to improve the reliability of measurements [32–36]. Nowadays, the increased detail of remote sensing satellite data products can provide information on moisture conditions in the first centimeters of soils, making available information helpful for defining runoff thresholds.

In this framework, the general objective of the present work is to investigate the possibility of using satellite soil moisture data to predict runoff thresholds, runoff and soil loss on an experimental plot (8 × 22 m) at the SERLAB experimental station (central Italy), characterized by fine fluvial-lacustrine deposits. The specific objectives are (i) to investigate the hydrologic response threshold values and dynamics with satellite soil moisture and rainfall data and (ii) to predict soil loss at the event scale with a USLE-MM model coupled with runoff models based on rainfall and satellite soil moisture data. Soil moisture data from Copernicus Sentinel-1 are integrated with data acquired on the ground (rainfall and runoff) at SERLAB. Runoff thresholds are presented by considering the seasonality and intensity of the events. Similar to the Scaife et al. [30] approach, the empirical runoff models below and above the thresholds are defined and coupled with the USLE-MM model to simulate the event of soil loss.

2. Materials and Methods

2.1. The SERLAB Experimental Station and the Runoff/Soil Loss Database

The Masse experimental station for soil erosion measurement of the Perugia University (SERLAB, Soil Erosion LABoratory, Figure 1) was established in 2007. It is located 20 km south of Perugia (42°59′34′′ N 12°17′27′′ E) in the Umbria region, central Italy. The station includes twelve plots:

- Four plots of 8 × 22 m^2;
- Two plots of 4 × 22 m^2;
- Two plots of 4 × 11 m^2;
- Two plots of 2 × 11 m^2;
- Two microplots of about 1 × 0.92 m^2.

Figure 1. View of the Masse experimental station, SERLAB (Central Italy). (42°59′34′′ N 12°17′27′′ E).

All plots are oriented parallel to a 16% slope. The area has a characteristic Mediterranean climate with an average annual rainfall of about 900 mm. The soil texture is silty-clay-loam (clay = 34%, silt = 59%, and sand = 7%) and the gravel content is negligible. The soil structure, massive when the soil is wet, becomes weak, fine, subangular, and blocky upon drying.

Each plot is equipped with a runoff collection system whose capacity (0.86 to 2.72 m^3) varies with the plot size. When a rainfall event producing runoff occurs, the collected volume is analyzed to measure the sediment concentration in the tanks and to derive the soil loss. All the plots (except for the first two on the right in Figure 1) are maintained in cultivated fallow through frequent tillage operations to remove any spontaneous vegetation and obliterate the presence of any rills formed during erosive events. The consistency of the data set is over 600 measures of event runoff and soil loss. Furthermore, the climatic station (tipping-bucket rain gauge, anemometer, thermometer, hygrometer) located within the experimental site provides the complete time series of climatic data since 2007 at a 5 min resolution. More details about the experimental schemes, technical features, and procedures of SERLAB can be found in previous papers [6,12–14,37,38]. For the study, only the data of one plot (8×22 m^2) were considered. This plot was equipped with a sonic distance sensor that enabled a detailed analysis of runoff formation and accumulation dynamics in the collecting tanks.

2.2. USLE Models for Soil Loss Estimation at the Event Scale

The original USLE equation for the estimation of the mean annual soil loss [8] has the following expression:

$$A = RKLSCP \tag{1}$$

where A (Mg ha^{-1} $year^{-1}$) is the mean annual soil loss per unit area, R = EI_{30} (MJ mm ha^{-1} h^{-1} $year^{-1}$) is the mean annual rainfall erosivity calculated as the product of the rainfall kinetic energy E (MJ ha^{-1}) by the maximum 30 min rainfall intensity observed during the event, I_{30} (mm h^{-1}), K (Mg ha h ha^{-1} MJ^{-1} mm^{-1}) is the soil erodibility factor, L (dimensionless) is the slope length factor, S (dimensionless) is the slope steepness factor, C (dimensionless) is the cover-management factor, and P (dimensionless) is the support practices factor.

Equation (1) can also be used to estimate the soil loss at event scale A_e (Mg ha^{-1}) using the erosivity factor of the single event R_e. A normalized value of the event soil loss $A_{e,N}$ can be obtained as:

$$A_{e,N} = \frac{A_e}{LSCP} = R_eK \tag{2}$$

Equation (2), however, tends to overestimate the lowest and underestimate the highest values [11]. The reason for this systematic error is the lack of explicit consideration of runoff. Various authors have proposed modifications to the USLE model to consider this aspect. The best-known models are the USLE-M, proposed by Kinnell and Risse [11], and the USLE-MM, proposed by Bagarello et al. [12]; both models include the runoff to correct the erosivity factor that becomes, actually, a rainfall runoff factor. The following expression can describe the two models:

$$A_{e,N} = (Q_R R_e)^{\alpha} K_u \tag{3}$$

where Q_R (mm/mm) is the event runoff coefficient, defined as the ratio of runoff volume Q (mm) and rainfall volume P (mm), with $\alpha = 1$ in the USLE-M and $\alpha > 1$ in the USLE-MM and where K_u is a modified erodibility factor that varies with the selected model.

The use of the USLE-MM model proved to be more efficient than the USLE-M model in the Italian experimental sites of Sparacia (Sicily) and Masse SERLAB [6]. In [6], based on the 532 measures of the SERLAB data set from 2008 to 2015, model (3) was parametrized with $K_u = 0.0896$ and $\alpha = 1.0479$. Other attempts were made in [14] that modified Equation (3) using soil moisture in place of the runoff coefficient in the rainfall runoff factor, deriving the model named Soil Moisture For Erosion, SM4E.

In this work, the possibility of using in the USLE-MM model the Q_R estimated by models based on the integrated use of satellite soil moisture data and event rainfall depth (i.e., $Q_R = f[(ADSI + P)]/P$) is evaluated and discussed. To focus the analysis on this objective, the USLE-MM model will be parametrized using the data selected in this study and deriving from the intersection of the SERLAB and Sentinel-1 data sets. The efficacy of the methodology is tested by comparing the estimated runoff, runoff coefficient, and soil loss with the corresponding measures available in the SERLAB data set.

2.3. Monitoring Soil Moisture from Satellite Data

The European Copernicus Project (Copernicus Global Land Service—CGLS), in service since 2013, aims to provide timely and high-quality essential bio-geophysical information and climate variables on the Earth′s surface on a global scale. The satellite product data (e.g., land surface temperature, water bodies area, vegetation index, soil moisture, etc.) make it possible to monitor the status and evolution of vegetation, energy cycles, and water on a global scale [39,40]. The Sentinel-1 mission comprises a constellation of two identical radar imagery satellites in the same orbit; Sentinel-1A was launched in April 2014 and Sentinel-1B in April 2016. Specifically, the Sentinel-1 SAR satellite sensor can derive the Copernicus Global Land SSM (Surface Soil Moisture) product that describes the soil moisture of the first 50 mm of soil on a 1 km (0.1°) spatial sampling. SSM1 km data are derived from observations using the model TU-Wien-Change-Detection [41–43]. Since January 2015, the Copernicus SSM 1 km product has been available for the European continent per individual location every 3–8 days, and since October 2016, every 1.5–4 days (thanks to Sentinel-1B satellite) in general. The SSM1 km products can be requested and downloaded free of charge from the website https://land.copernicus.eu/global/products/ssm (accessed on 10 January 2022), with the following naming standard: c_gls_SSM1 km_<YYYYMMDDHHMM>_CEURO_S1CSAR_<VX.Y.Z>.nc., where <YYYYMMDDHHMM> gives the temporal location of the file. The SSM1 km products include a netCDF4 file containing full resolution bands (ssm and ssm_noise), an XML file containing the metadata, and a colored geo-tiff file.

Sentinel-1 derives SSM(t) (Surface Soil Moisture at t time) directly from the observed radar backscatter; the changes in backscatter are interpreted as changes in soil moisture, while other surface properties such as geometry and roughness, and vegetation structure are interpreted as static parameters. The incidence angle dependency of the backscatter is modeled by the linear slope parameter, which allows normalization to a common reference observation angle (θr = 40°). The model parameters describe maximum dry and wet conditions and average signal contributions from vegetation and surface geometry. The long-term backscatter measurements are used to derive dry and wet soil conditions (parameters $\sigma^0{}_{dry(40)}$ and $\sigma^0{}_{wet(40)}$) from the radar backscatter signal [44]. The relative surface soil moisture is given by:

$$\mathrm{SSM(t)} = \frac{\sigma_{40}(\mathrm{t}) - \sigma^0_{\mathrm{dry(40)}}}{\sigma^0_{\mathrm{wet}} - \sigma^0_{\mathrm{dry}}} \tag{4}$$

SSM(t) represents a degree of saturation and ranges between 0% and 100% [40]. The volumetric water content $\mathrm{SSM_a(t)}$ can be obtained by introducing the soil porosity (n) as follows:

$$\mathrm{SSM_a(t)} = \mathrm{n}\frac{\mathrm{SSM(t)}}{100} \tag{5}$$

As reported in the introduction, identifying runoff thresholds by empirical approaches requires the knowledge of the antecedent soil moisture content, i.e., $\mathrm{SSM_a(t)}$ at the time (t) just before the rainfall event triggering runoff. Since the first centimeters of soil layers are often tilled and, therefore, the porosity is very variable in space and time [45–47], obtaining $\mathrm{SSM_a(t)}$ values from SSM(t) is not possible. In other words, $\mathrm{SSM_a(t)}$ values obtained by Equation (5) may not be reliable. A possible way to overcome this problem is using SSM(t) satellite data to calculate the Antecedent Degree of Saturation Index (ADSI) similarly to ASI in [21]:

$$\mathrm{ADSI} = \mathrm{h}\frac{\mathrm{SSM(t)}}{100} \tag{6}$$

where h is the thickness of the investigated soil, which is the first 50 mm for satellite observations, and ADSI is expressed in mm.

For this investigation, the SERLAB data set overlapped with the SSM1 km data by Copernicus Sentinel-1 available from January 2015. Considering that SSM(t) data are not continuous, only rainfall runoff events that occurred concurrently or just after the satellite SSM(t) measures were selected for the analysis.

3. Results

3.1. SERLAB Data Set

Forty-seven measurements were captured by overlapping the SSM1km Copernicus Sentinel-1 and the SERLAB data set; eighteen correspond to rainfall events that did not produce runoff, and three lacked soil loss measures. Table S1 shows the information available for the crossing set of data. From the SERLAB data set, the rainfall depth (P), runoff event (Q), and the soil loss, A_e, for the erosive events and other rainfall characteristics along with the corresponding date of occurrence are extracted. From Copernicus Sentinel-1, the corresponding SSM values with the date of satellite data acquisitions are extracted.

Most runoff values are lower than 2.0 mm (about 83% of the observations), while the others are higher than 5 mm, with a maximum value of 15.5 mm. The no runoff events (about 38% of the observation) have rainfall depth, P, lower than 10.0 mm, while the runoff, along with the soil loss, occurs for rainfall higher than 18.8 mm. Overall, the maximum P is about 87.4 mm, with a mean value of 30.4 mm. Six runoff events occurred with antecedent SSM(t) higher than 80%, one of which contributed to producing the highest runoff and erosive event during the autumn–winter season coupled with a cumulated rainfall of about 68.8 mm. The maximum rainfall intensity in 30 min, I_{30}, varies between 2.0 and 54.0 mm/h, with three events over 40.0 mm/h and soil loss values higher than 17.0 t/ha. These events in the data set are surveyed as rill events while the others are classified as interrill.

3.2. Definition of the Relationship between the Runoff and the ADSI + P

The rainfall data compared with the runoff values measured at SERLAB since 2008 consist of about a hundred measures (Figure 2a). Data points for which Copernicus SSM1km data are available (Table S1) are highlighted in Figure 2a. As expected, P values do not explain the runoff processes alone (i.e., for the same rainfall event, different runoff values correspond). Hence it is impossible to derive an accurate mathematical relationship estimating runoff from rainfall only. Therefore, when available, we tried to improve the runoff prediction model by correcting the rainfall depth with the antecedent soil moisture conditions. Although the consistency of the database is drastically reduced (47 measurements), a first attempt to improve the runoff estimation was carried out. Similar to the widely used approach that relates runoff and (ASI + P), the runoff values have been associated with ADSI + P (Figure 2b). Multiple thresholds are highlighted under the hypothesis that the data set can be classified on the basis of the season of occurrence. By separating the data set into the autumn–winter and the spring–summer events and according to [29], it is possible to identify the generation threshold (occurring at ADSI + P = 38.0 mm), the rise threshold for spring–summer events (ADSI + P = 63.2 mm), and the rise threshold for autumn–winter events (ADSI + P = 93.2 mm). In this analysis generation threshold corresponds to the ADSI + P value triggering runoff, while rise thresholds identify the ADSI + P values when the runoff behavior changes mainly due to the specific characteristics of the rainfall graph. Therefore, the rise thresholds separate events in high from the low hydrological response. A single linear model has been fitted to the events with low runoff (lower than 2.0 mm) to obtain an empirical relationship between ADSI + P and the runoff. Although runoff events higher than 2.0 mm are few, straight lines are used to describe the high runoff events maintaining the seasonal classification. This procedure seems to be viable even if, in this case, the few data available do not provide certainty that the hypothesis is reliable. The regressions models that are also drawn in Figure 2b, are as follows:

- For autumn–winter events

$$Q = 0.0188\ (ADSI + P) - 0.503\ 38.0 < ADSI + P < 93.2\ R^2 = 0.390 \tag{7a}$$

$$Q = 0.814\ (ADSI + P) - 75.826\ 93.2 \leq ADSI + P < 109.0\ R^2 = 0.934 \tag{7b}$$

- For spring–summer events

$$Q = 0.0188\ (ADSI + P) - 0.503\ 38.0 < ADSI + P < 63.2\ R^2 = 0.39 \tag{8a}$$

$$Q = 0.425\ (ADSI + P) - 26.823\ 63.2 \leq ADSI + P < 84.0\ R^2 = 0.824 \tag{8b}$$

The analysis indicates that some spring–summer events cannot be explained only by the ADSI + P approach (the three events indicated with triangles in Figure 2b). These three events are classified as rill in the SERLAB data set (Table S1) and have not been included in the regression analysis to determine the models given in Equations (7a,b) and (8a,b). This choice is discussed later in the paper. Moreover, few events behave differently, deviating from the linear regression models proposed. For example, point no. 15 in Figure 2b (occurring in September 2016, Table S1) provides a low runoff than that predicted by the spring–summer rise threshold model (Equation (8b)); the point no. 22 (occurring in May 2018, Table S1) is among the spring–summers but behaves like the autumn–winter ones. This latter event is characterized by one of the most prolonged duration (12.33 h), and it is preceded by very wet soil conditions (SSM(t) = 76%).

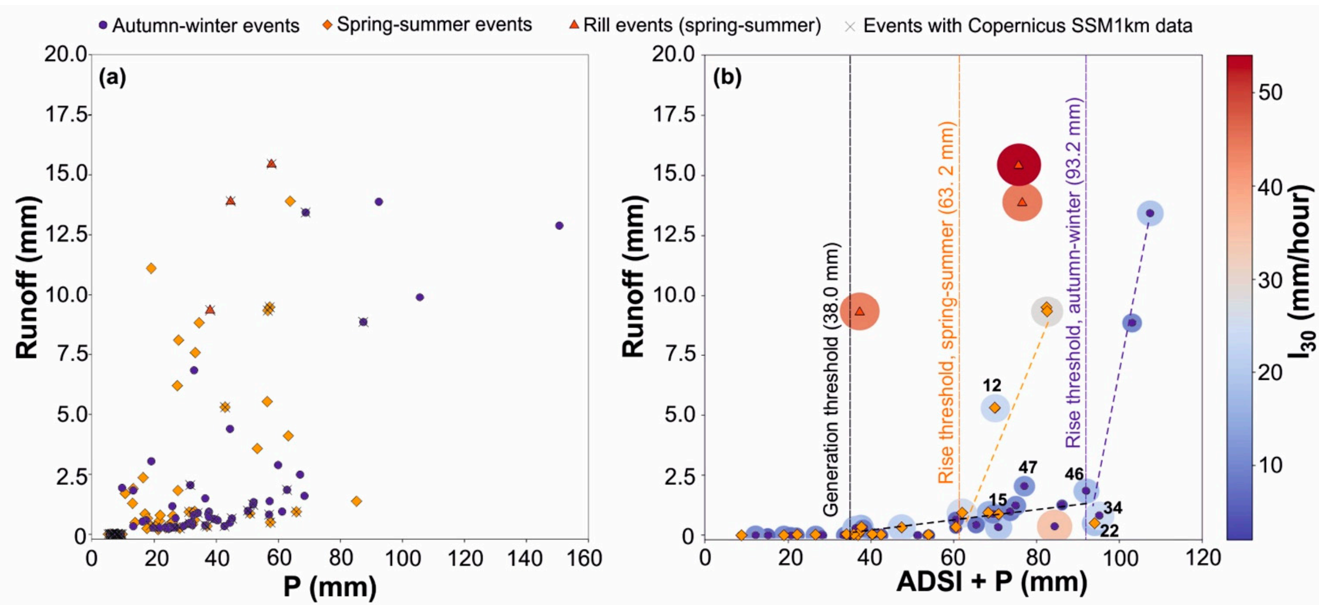

Figure 2. Runoff events separated into spring–summer and autumn–winter periods. (**a**) Runoff vs. event rainfall depth (P) for the 2008–2020 period; (**b**) Runoff vs. the sum of Antecedent Degree of Saturation Index and P (ADSI + P), with generation threshold and rise thresholds for the two periods (only events with Copernicus SSM1km data available are considered, Table S1). The numbers associated with some selected events in Figure 2b refer to Table S1.

3.3. Estimation of the Runoff, Runoff Coefficient, and the Soil Loss

The functions Q = f (ADSI + P) given in Figure 2b (Equations (7a,b) and (8a,b)) have been used to estimate the runoff (Q) from ADSI data and the gauging station P records. The comparison between the estimated and measured runoff (Table S1) is given in Figure 3a. In Figure 3b, the same comparison is presented in terms of runoff coefficients (Q_R).

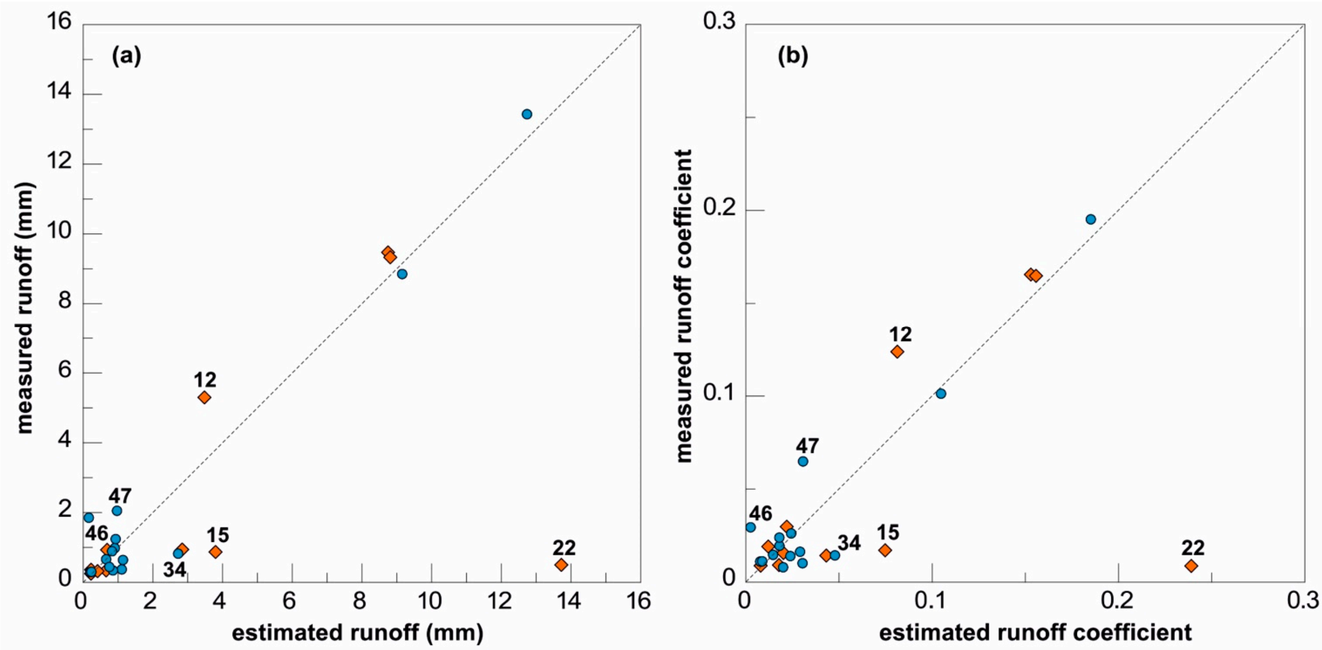

Figure 3. Comparison between the measured runoff and the runoff estimated by the models Q = f (ADSI + P), Equations (7a,b) and (8a,b) (**a**); same comparison based on the runoff coefficient (**b**). Blue dots and orange diamonds indicate autumn–winter and spring–summer events, respectively. The numbers associated with some selected events referred to in Table S1.

The highest estimation errors derive from the events nos. 15 and 22 (Table S1). Although these events have ADSI + P values higher than the rise threshold ones, the measured runoff is lower than those estimated by steeper linear models. The root mean square errors (RMSE) associated with the estimated runoff (Figure 3a) are 0.8, 4.17, and 2.78 mm, for the autumn–winter, spring–summer, and overall data set, respectively. The RMSE obtained for the spring–summer, and overall data sets are very negatively affected by events 15 and 22 (Figure 3) already mentioned above in the paper. However, even excluding these events, the RMSE for spring–summer events becomes 2.0 mm, remaining higher than autumn–winter events. Similar considerations can be made for the runoff coefficient (Figure 3b). In this case, the RMSEs for the different data sets are 0.02, 0.07, and 0.05 for the autumn–winter, spring–summer, and overall data sets, respectively (average 2.14 mm).

The 27 events for which the soil loss measures are available (Table S1) are used to parametrize a USLE-MM model. This model is optimized for this study but is not to be intended as representative of the full SERLAB data set (2008–2020).

Referring to the parametrized USLE-MM model (Equation (3)), the regression analysis in Figure 4 for the data set in Table S1 gives Equation (9).

$$A_{e,N} = 0.0317(Q_R R_e)^{1.1038} \tag{9}$$

Using Equation (9), with the Q_R values calculated as the ratio between the runoff calculated from the satellite and rainfall data (Q = f (ADSI + P), Equations (7a,b) and (8a,b)), and the corresponding P, the normalized soil loss $A_{e,N}$ was estimated. Figure 5 compares these $A_{e,N}$ values and those estimated by Equation (9) using the measured Q_R (Table S1). Most events are distributed around the 1:1 line, thus indicating a moderate effect on the USLE-MM model prediction by using a Q_R estimated by satellite and rainfall data instead of the measured one. The role of the season does not appear particularly marked. In addition, in this case, the estimation errors are very negatively affected by the events commented on above in the paper. In particular, for the event no. 22, there is a relevant overestimation of the soil loss deriving from the estimated runoff. Events nos. 15 and 34 provide the same kind of error, although less. Opposite consideration can be done for the events nos.

12, 47, and 46. The graph in Figure 5 is bi-logarithmic to visualize better the low events otherwise grouped around the origin of the axes. Meanwhile, this representation enables one to appreciate the goodness of fit of the higher values of soil loss, which greatly affects the quantification of the erosion process over a long period.

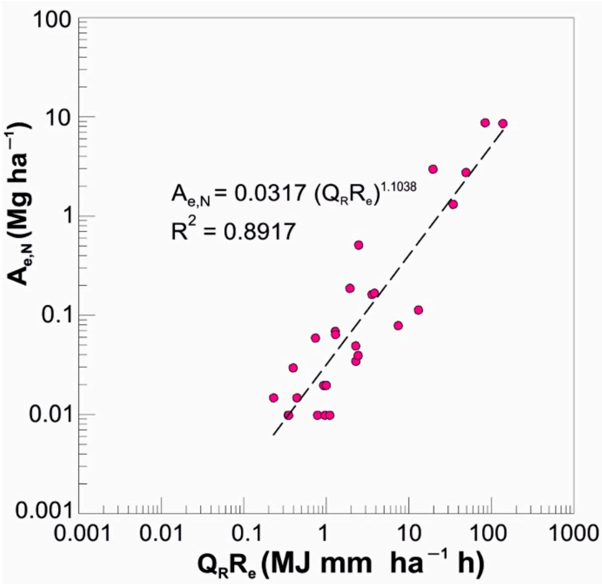

Figure 4. Scatter plots of the measured pairs (Q_RR_e, $A_{e,N}$) and USLE-MM model (equation in the graph) for the data set given in Table S1.

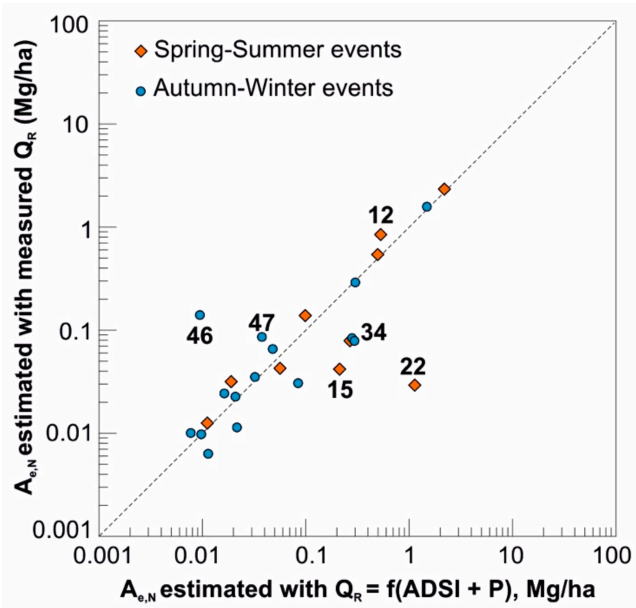

Figure 5. Comparison between the soil loss estimated by Equation (4) with the Q_R measured and estimated as the ratio between the runoff, Q = f (ADSI + P), Equations (7a,b) and (8a,b), and the corresponding measured rainfall P. Blue dots and orange diamonds indicate autumn–winter and spring–summer events, respectively. The numbers associated with some selected events are referred to in Table S1.

The estimation error of the runoff and runoff coefficient results in a noticeable worsening of soil loss estimation. In Figure 6, the observed values $A_{e,N}$ are compared with those estimated by the USLE-MM model (Equation (9)) in two conditions: with Q_R measured and with Q_R derived from satellite and rainfall data (Q = f (ADSI + P) by using Equation (7a,b) for autumn–winter events, Equation (8a,b), for spring–summer events.

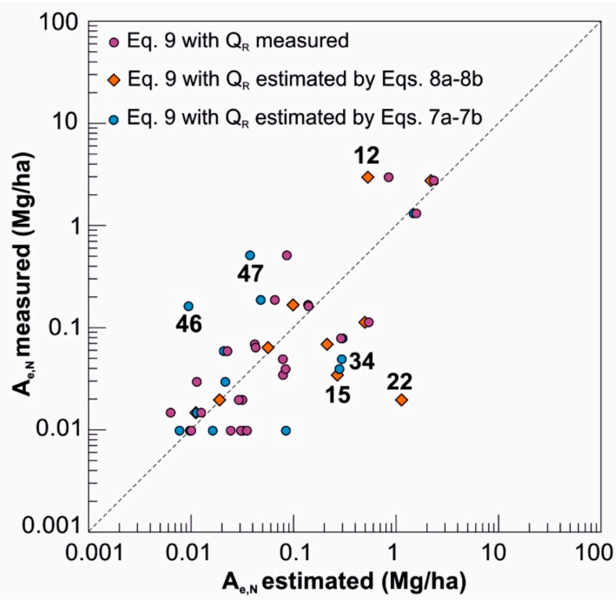

Figure 6. Goodness of fit of the soil loss measured and estimated by the USLE-MM model (Equation (9)) with Q_R measured and estimated by Equations (7a,b) and (8a,b). Blue dots and orange diamonds indicate autumn–winter and spring–summer events, respectively. The numbers associated with some selected events are referred to in Table S1.

In terms of RMSE, the estimation errors are similar, 0.46 and 0.57 t/ha, respectively, but as expected, are higher when the ADSI + P data are used to calculate the runoff instead of Q_R measured. In addition, in this case, the results are very negatively affected by the events with nos. 12, 15, 22, 34, 46, and 47 (Table S1).

4. Discussion

The data set used for the analysis included events with records of satellite soil water content (expressed by the index ADSI), and rainfall (P), runoff (Q), rainfall erosivity (R_e), soil loss (A_e) measured at plot scale (SERLAB experimental field). Four different behaviors can be identified when plotting the points in a cartesian plane (Q vs. ADSI + P, Figure 2b). First of all, the three events classified as rill in the SERLAB data set show behavior on their own, with a very high hydrological response (runoff and soil loss) at a medium ADSI + P value. A specific model describing rill events has not been built due to the small data set. Classifying of the events in rill/interrill is also possible according to specific activation thresholds [48,49] based only on widely available rainfall graph characteristics. In particular, the three recognized rill events are characterized by R_e values (Table S1) higher than or very close to the value R_e = 359 mm ha^{-1} h^{-1} proposed in [49] as the threshold for the rill erosion process activation at the SERLAB. In addition, in terms of I_{30}, these events differentiate from the others (Table S1, Figure 2b).

Another group of five events (nos. 1, 4, 12, 26, and 45 in Table S1) shows an intermediate hydrological response (runoff and soil loss) at a medium ADSI + P. Three of them enable the determination of the summer-spring relationship above the rise threshold (Equation (8b)) and the other two the analogous line for the winter-autumn period (Equation (7b)). In addition, in this case, it is possible to explain the specific behavior of this group in terms of hydrological response, mainly based on the characteristics of the rainfall graph. The two events intercepted by the autumn–winter rise (nos. 26 and 45) are characterized by mean intensity (IM), generally much lower than the events belonging to the spring–summer rise (nos. 1, 4, and 12). An exception is represented by event no. 4, which has an I_M only slightly higher than those of events 26 and 45. However, a detailed analysis of the rainfall graphs of the spring–summer events (nos. 1, 4, and 12) revealed that these consist almost entirely of a single shower ("burst") to which more than 90% of rain belongs.

Autumn–winter events, instead, have their total precipitation distributed in numerous showers. Evidently, events with higher IM and more concentrated volumes over time (as typically occurs for summer events) can lead to a more rapid decay of the infiltration rate and an earlier occurrence of the runoff with the same ADSI + P. The last two groups show, respectively, null runoff response at low ADSI + P and low hydrological response (runoff and soil loss) at a medium ADSI + P. The models predicting Q from ADSI + P data were derived based on this classification. The segmented linear regression models with a low slope for low hydrological response and a high slope for high hydrological response, in the literature, are named "hockey stick" behavior [23] and seem the most appropriate to describe the relationship between the ADSI + P and Q in the database analyzed. A different hockey stick model was associated with "spring–summer" and "autumn–winter" groups, respectively, with a higher rise threshold for the latter.

The performance of the Q = f (ADSI + P) models is fairly satisfactory, estimating quite accurately both the low and high runoff (Figure 3). This result is very important as the most intense events, although rare, are those that produce the greatest runoff and soil loss. It is widely recognized [6,10] that the annual soil loss is produced almost entirely by a few very intense events that modify the hydrological connectivity and drag downstream the detached material only partially displaced by less intense events.

This fact results in a pretty suitable estimate of the event soil loss when the runoff simulated with the inferred models is used to input the USLE-MM (Equation (9)). As expected, the USLE-MM model provides a less accurate estimate with a slightly higher RMSE (0.57) if compared with the performance obtained using the measured Q_R (RMSE = 0.49) with a more scattered point cloud (Figure 6). However, the benchmark for the correct assessment of the USLE-MM (Equation (9)) with runoff coefficient derived from satellite and rainfall data ADSI + P is the performance of USLE-derived models that include predicted runoff coefficient [14,15,50]. Todisco et al. [14], analyzing a SERLAB database of about 60 plot soil loss values (average 3.5 Mg/ha) and the estimated soil loss by a USLE-MM model coupled with MISDc model [51], found RMSE = 2.96 Mg/ha. We obtain a moderately worse result by using the Q values obtained by the presented models (Equations (7a,b) and (8a,b)) in Equation (9): RMSE 0.57 Mg/ha compared to an average of 0.35 Mg/ha.

Furthermore, the differentiation of the rainfall runoff models according to the season (autumn–winter and spring–summer) agrees with the results obtained by [14] when stating that the hydrological behavior is different for summer and winter rainfalls due to the particular characteristics of summer rainfall events in central Europe [48]. As a consequence, the performance in the estimation of the soil loss differs whether evaluated for the entire data set or separately for the two seasons, being much better for the autumn–winter period. The small database considered and the resulting uncertainty about the "hockey stick" relationships identified may certainly have negatively affected the results.

Due to the small data set available, we used all data to create the predictive relationships, representing the main weak point of the analysis. Hence, it was impossible to validate the relationships using an independent data set. Unfortunately, in recent years, in which satellite data are available, few rainy events were able to produce runoff and soil loss at SERLAB. Therefore, the relationships derived (Equations (7a,b) and (8a,b)) and the actual contribution of the antecedent soil water content in the accuracy of runoff prediction has to be considered as a preliminary result. The study aims mainly to show the concept, which will have to be confirmed with further measures. On the other hand, runoff is a very complex process depending on several components such as locally specific rainfall, crop and soil use, soil conditions, and slope [52]. In this context, the satellite moisture data, even at low resolutions, can represent an explanatory variable helpful in improving the accuracy of the runoff estimate, especially when in-field monitoring data are unavailable. This is demonstrated by the growing use of Copernicus SSM1km data for hydrological applications, even at the slope scale [14,53–55].

Furthermore, it is necessary to underline that the performance obtained is better than that provided by the original USLE model, which is still the most widely used model for estimating soil loss, given the difficulty in measuring runoff. In fact, by applying the USLE model (Equation (2)) with the soil erodibility factor K = 0.02 estimated from the SERLAB database (2008–2020), we obtain for the data set of Table S1 an RMSE $\approx$ 3.1 Mg/ha that is much higher than the value (RMSE 0.57 Mg/ha) derived using Q = f (ADSI + P) in Equation (9). Therefore, using a USLE-MM model (albeit with remote estimated runoff data) is still advantageous at the event scale compared to the USLE model, which does not consider the runoff.

5. Conclusions

The work analyzed the Masse SERLAB data set of erosive and non-erosive events, jointly with that derived from Copernicus Sentinel-1 of surface soil moisture (from 2015 onward). The events simultaneously present in the two data sets were extracted and analyzed. For these events, we have all the erosion data: soil loss (A_e), runoff event (Q), runoff coefficient (Q_R), and rainfall data (P, I_{30}, R_e), and at the same time, the surface soil moisture (SSM) and the corresponding Antecedent Degree of Saturation Index (ADSI) in the first 50 mm of the soil. The data set was analyzed with the dual purpose of verifying the possibility of identifying a relationship between ADSI + P and Q and evaluating the possibility of using these models to estimate the runoff Q and the corresponding runoff coefficient QR. The estimated runoff coefficient has also been used in a USLE-MM model to estimate the soil loss event. The following findings were achieved:

1. As expected, the event rainfall depth (P), if corrected with the corresponding ADSI value, does explain the runoff process reasonably well, at least with the available data;
2. By separating the data set into the autumn–winter and the spring–summer events, it is possible to identify the generation threshold (ADSI + P value triggering runoff) and the rise thresholds (ADSI + P values at which the runoff behavior changes, Table S1);
3. The relationship Q = f (ADSI + P) was derived for spring–summer events and autumn–winter events (Equations (7a,b) and (8a,b));
4. Using a USLE-MM model (albeit with remote estimated runoff data) is still advantageous at the event scale compared to the USLE model.

The small database considered and the resulting uncertainty about the relationships identified may certainly have negatively affected the result. The database used is not large enough to interpret the results correctly. In particular, there is a double open question: the events that it was possible to analyze (as they fall within the temporal intersection of the two databases) are few in absolute terms; furthermore, the number of rill data is low in the Masse SERLAB data set, and this prevented an overall assessment of events with high runoff. Future developments could use other erosion databases to make the analysis more robust.

We highlight that the obtained results open interesting scenarios in the overview of the studies aimed at defining USLE-derived models that could improve the unit soil loss estimation at the event scale. In particular, the choice of using SSM data to estimate the runoff is very important for the practice. Moreover, remote sensing soil moisture data are widely available globally. Satellite data shows the potential of applying the developed USLE-derived model for large-scale monitoring and quantification of the soil erosion process.

Supplementary Materials: The following supporting information can be downloaded at: https://www.mdpi.com/article/10.3390/w14132081/s1, Table S1. SERLAB and Sentinel-1 databases of rainfall, runoff and antecedent soil moisture observations.

Author Contributions: Conceptualization, F.T. and L.D.M.; methodology, F.T. and L.D.M.; validation, L.V. and S.O.; investigation, F.T. and L.V.; formal analysis, resources, data curation, writing, F.T., L.V., L.D.M., and S.O.; funding acquisition, F.T., L.V. All authors have read and agreed to the published version of the manuscript.

Funding: This work was funded by the 'Ricerca di Base, 2019′ project, University of Perugia - Italy (principal investigator Francesca Todisco) and 'Ricerca di Base, 2017′ project, University of Perugia - Italy (principal investigator Lorenzo Vergni).

Data Availability Statement: All the data used in the work are available in Table S1.

Conflicts of Interest: The authors declare no conflict of interest.

References

1. Bisantino, T.; Bingner, R.; Chouaib, W.; Gentile, F.; Trisorio, L.G. Estimation of runoff, peak discharge and sediment load at the event scale in a medium-size Mediterranean watershed using the ANNAGNPS model. *Land Degrad. Dev.* **2015**, *26*, 340–355. [CrossRef]
2. Borrelli, P.; Märker, M.; Schütt, B. Modelling post-tree-harvesting soil erosion and sediment deposition potential in the Turano River basin (Italian Central Apennine). *Land Degrad. Dev.* **2015**, *26*, 356–366. [CrossRef]
3. Foster, G.R.; Toy, T.E.; Renard, K.G. Comparison of the USLE, RUSLE1.06 and RUSLE2 for application to highly disturbed lands. *First Interag. Conf. Res. Watersheds* **2003**, *27*, 154–160.
4. Borrelli, P.; Robinson, D.A.; Fleischer, L.R.; Lugato, E.; Ballobio, C.; Alewell, A.; Meusburger, K.; Modugno, S.; Schutt, B.; Ferro, V.; et al. An assessment of the global impact of 21st century land use change on soil erosion. *Nat. Commun.* **2017**, *8*, 2013. [CrossRef]
5. Panagos, P.; Ballabio, C.; Borrelli, P.; Meusburger, K.; Klik, A.; Rousseva, S.; Tadić, M.P.; Michaelides, S.; Hrabalíková, M.; Olsen, P.; et al. Rainfall erosivity in Europe. *Sci. Total Environ.* **2015**, *511*, 801–814. [CrossRef]
6. Bagarello, V.; Ferro, V.; Pampalone, V.; Porto, P.; Todisco, F.; Vergni, L. Predicting soil loss in central and south Italy with a single USLE-MM model. *J. Soils Sediments* **2018**, *18*, 3365–3377. [CrossRef]
7. Ganasri, B.P.; Ramesh, H. Assessment of soil erosion by RUSLE model using remote sensing and GIS-a case study of Nethravathi Basin. *Geosci. Front.* **2016**, *7*, 953–961. [CrossRef]
8. Wischmeier, W.H.; Smith, D.D. *Predicting Rainfall-Erosion Losses: A Guide to Conservation Farming*; U.S. Department of Agriculture, Science and Education Administration: Washington, DC, USA, 1978; p. 537.
9. Larson, W.E.; Lindstrom, M.J.; Schumacher, T.E. The role of severe storms in soil erosion: A problem needing consideration. *J. Soil Water Conserv.* **1997**, *52*, 90–95.
10. Di Stefano, C.; Pampalone, V.; Todisco, F.; Vergni, L.; Ferro, V. Testing the Universal Soil Loss Equation-MB equation in plots in Central and South Italy. *Hydrol. Processes* **2019**, *33*, 2422–2433. [CrossRef]
11. Kinnell, P.I.A.; Risse, L.M. USLE-M: Soil Empirical modeling rainfall erosion through runoff and sediment concentration. *Sci. Soc. Am. J.* **1998**, *62*, 1667–1672. [CrossRef]
12. Bagarello, V.; Di Piazza, G.V.; Ferro, V.; Giordano, G. Predicting unit plot soil loss in Sicily, south Italy. *Hydrol. Processes* **2008**, *22*, 586–595. [CrossRef]
13. Bagarello, V.; Ferro, V.; Pampalone, V.; Porto, P.; Todisco, F.; Vergni, L. Statistical check of USLE-M and USLE-MM to predict bare plot soil loss in two Italian environments. *Land Degrad. Dev.* **2018**, *18*, 3365–3377. [CrossRef]
14. Todisco, F.; Brocca, L.; Termite, L.F.; Wagner, W. Use of satellite and modeled soil moisture data for predicting event soil loss at plot scale. *Hydrol. Earth Syst. Sci.* **2015**, *19*, 3845–3856. [CrossRef]
15. Gao, G.Y.; Fu, B.J.; Lü, Y.H.; Liu, Y.; Wang, S.; Zhou, J. Coupling the modified SCS-CN and RUSLE models to simulate hydrological effects of restoring vegetation in the Loess Plateau of China. *Hydrol. Earth Syst. Sci.* **2012**, *16*, 2347–2364. [CrossRef]
16. Kinnell, P.I.A. Modelling event soil losses using the QREI30 index within RUSLE2. *Hydrol. Processes* **2014**, *28*, 2761–2771. [CrossRef]
17. McGlynn, B.L.; McDonnell, J.J. Quantifying the relative contributions of riparian and hillslope zones to catchment runoff. *Water Resour. Res.* **2003**, *39*, 1310. [CrossRef]
18. Thomaz, E.L. The influence of traditional steep land agricultural practices on runoff and soil loss. *Agric. Ecosyst. Environ.* **2009**, *130*, 23–30. [CrossRef]
19. Detty, J.M.; McGuire, K.J. Threshold changes in storm runoff generation at a till-mantled headwater catchment. *Water Resour. Res.* **2010**, *46*, W07525. [CrossRef]
20. Scaife, C.I.; Band, L.E. Nonstationarity in threshold response of stormflow in southern Appalachian headwater catchments. *Water Resour. Res.* **2017**, *53*, 6579–6596. [CrossRef]
21. Haga, H.; Matsumoto, Y.; Matsutani, J.; Fujita, M.; Nishida, K.; Sakamoto, Y. Flow paths, rainfall properties, and antecedent soil moisture controlling lags to peak discharge in a granitic unchanneled catchment. *Water Resour. Res.* **2005**, *41*, W12410. [CrossRef]
22. Penna, D.; Tromp-van Meerveld, H.J.; Gobbi, A.; Borga, M.; Dalla Fontana, G. The influence of soil moisture on threshold runoff generation processes in an alpine headwater catchment. *Hydrol. Earth Syst. Sci.* **2011**, *15*, 689–702. [CrossRef]
23. Ali, G.; Oswald, C.J.; Spence, C.; Cammeraat, E.L.; McGuire, K.J.; Meixner, T.; Reaney, S.M. Towards a unified threshold-based hydrological theory: Necessary components and recurring challenges. *Hydrol. Processes* **2013**, *27*, 313–318. [CrossRef]
24. Weiler, M.; McDonnell, J.J.; Tromp-van Meerveld, I.; Uchida, T. Subsurface stormflow. *Encycl. Hydrol. Sci.* **2006**, 1–14. [CrossRef]
25. Tromp-van Meerveld, H.J.; McDonnell, J.J. Threshold relations in subsurface stormflow: 1. A 147-storm analysis of the Panola hillslope. *Water Resour. Res.* **2006**, *42*, 1–11. [CrossRef]

26. James, A.L.; Roulet, N. Investigating hydrologic connectivity and its association with threshold change in runoff response in a temperate forested watershed. *Hydrol. Processes* **2007**, *21*, 3391–3408. [CrossRef]
27. Zehe, E.; Elsenbeer, H.; Lindenmaier, F.; Schulz, K.; Blöschl, G. Patterns of predictability in hydrological threshold systems. *Water Resour. Res.* **2007**, *43*, W07434. [CrossRef]
28. Penna, D.; van Meerveld, H.J.; Oliviero, O.; Zuecco, G.; Assendelft, R.S.; Dalla Fontana, G.; Borga, M.A.R.C.O. Seasonal changes in runoff generation in a small forested mountain catchment. *Hydrol. Processes* **2015**, *29*, 2027–2042. [CrossRef]
29. Wei, L.; Qiu, Z.; Zhou, G.; Kinouchi, T.; Liu, Y. Stormflow threshold behaviour in a subtropical mountainous headwater catchment during forest recovery period. *Hydrol. Processes* **2020**, *34*, 1728–1740. [CrossRef]
30. Scaife, C.I.; Singh, N.K.; Emanuel, R.E.; Miniat, C.F.; Band, L.E. Non-linear quickflow response as indicators of runoff generation mechanisms. *Hydrol. Processes* **2020**, *34*, 2949–2964. [CrossRef]
31. Wang, S.; Yan, Y.; Fu, Z.; Chen, H. Rainfall-runoff characteristics and their threshold behaviors on a karst hillslope in a peak-cluster depression region. *J. Hydrol.* **2021**, *605*, 127370. [CrossRef]
32. Vaz, C.M.; Jones, S.; Meding, M.; Tuller, M. Evaluation of standard calibration functions for eight electromagnetic soil moisture sensors. *Vadose Zone J.* **2013**, *12*, 1–16. [CrossRef]
33. Di Matteo, L.; Pauselli, C.; Valigi, D.; Ercoli, M.; Rossi, M.; Guerra, G.; Cambi, C.; Ricco, R.; Vinti, G. Reliability of water content estimation by profile probe and its effect on slope stability. *Landslides* **2018**, *15*, 173–180. [CrossRef]
34. Kargas, G.; Londra, P.; Anastasatou, M.; Moustakas, N. The effect of soil iron on the estimation of soil water content using dielectric sensors. *Water* **2020**, *12*, 598. [CrossRef]
35. Di Matteo, L.; Spigarelli, A.; Ortenzi, S. Processes in the Unsaturated Zone by Reliable Soil Water Content Estimation: Indications for Soil Water Management from a Sandy Soil Experimental Field in Central Italy. *Sustainability* **2021**, *13*, 227. [CrossRef]
36. Ortenzi, S.; Mangoni, M.; Di Matteo, L. Estimating moisture content and hydraulic properties of unsaturated sandy soils of Tiber River (Central Italy): Integrating data from calibrated PR2/6 probe and hydraulic property estimator. *Acque Sotter.—Ital. J. Groundw.* **2022**, *11*, 17–25. [CrossRef]
37. Bagarello, V.; Ferro, V.; Giordano, G.; Mannocchi, F.; Pampalone, V.; Todisco, F.; Vergni, L. Effect of plot size on measured soil loss for two Italian experimental sites. *Biosyst. Eng.* **2011**, *108*, 18–27. [CrossRef]
38. Todisco, F.; Vergni, L.; Mannocchi, F.; Bomba, C. Calibration of the soil loss measurement method at the Masse experimental station. *Catena* **2012**, *91*, 4–9. [CrossRef]
39. Doubkova, M.; Wagner, W.; Naeimi, V.; Cao, S.; Bauer-Marschallinger, B.; Kidd, R.; Hasenauer, S.; Dostalova, A.; Paulik, C. The use of Sentinel-1 for monitoring of soil moisture within the copernicus global land service. *Living Planet Symp.* **2016**, *740*, 105.
40. Copernicus Global Land Operations. Available online: https://land.copernicus.eu/global/sites/cgls.vito.be/files/products/CGLOPS1_PUM_SSM1km-V1_I1.30.pdf (accessed on 16 February 2022).
41. Wagner, W. Soil Moisture Retrieval from ERS Scatterometer Data. Institut für Photogrammetrie u. Fernerkundung d. Technologie University: Karlsruhe, Germany, 1998; p. 49.
42. Wagner, W.; Lemoine, G.; Rott, H. A method for estimating soil moisture from ERS scatterometer and soil data. *Remote Sens. Environ.* **1999**, *70*, 191–207. [CrossRef]
43. Hornacek, M.; Wagner, W.; Sabel, D.; Truong, H.L.; Snoeij, P.; Hahmann, T.; Diedrich, E.; Doubková, M. Potential for high resolution systematic global surface soil moisture retrieval via change detection using Sentinel-1. *IEEE J. Sel. Top. Appl. Earth Obs. Remote Sens.* **2012**, *5*, 1303–1311. [CrossRef]
44. Bauer-Marschallinger, B.; Freeman, V.; Cao, S.; Paulik, C.; Schaufler, S.; Stachl, T.; Modanesi, S.; Massari, C.; Ciabatta, L.; Brocca, L.; et al. Toward global soil moisture monitoring with Sentinel-1: Harnessing assets and overcoming obstacles. *IEEE Trans. Geosci. Remote Sens.* **2018**, *57*, 520–539. [CrossRef]
45. Richard, G.; Cousin, I.; Sillon, J.F.; Bruand, A.; Guérif, J. Effect of compaction on the porosity of a silty soil: Influence on unsaturated hydraulic properties. *Eur. J. Soil Sci.* **2001**, *52*, 49–58. [CrossRef]
46. Fu, Y.; Tian, Z.; Amoozegar, A.; Heitman, J. Measuring dynamic changes of soil porosity during compaction. *Soil Tillage Res.* **2016**, *193*, 114–121. [CrossRef]
47. de Oliveira, J.A.; Cássaro, F.A.; Pires, L.F. Estimating soil porosity and pore size distribution changes due to wetting-drying cycles by morphometric image analysis. *Soil Tillage Res.* **2021**, *205*, 104814. [CrossRef]
48. Todisco, F. The internal structure of erosive and non-erosive storm events for interpretation of erosive processes and rainfall simulation. *J. Hydrol.* **2014**, *519*, 3651–3663. [CrossRef]
49. Todisco, F.; Vergni, L.; Vinci, A.; Pampalone, V. Practical thresholds to distinguish erosive and rill rainfall events. *J. Hydrol.* **2019**, *579*, 124173. [CrossRef]
50. Todisco, F.; Brocca, L.; Mannocchi, F.; Melone, F.; Moramarco, T. Using continuous hydrological modeling coupled to a modified USLE model for predicting plot soil loss in Umbria. In *Quaderni di Idronomia Montana*; Edibios: Cosenza, Italy, 2012; Volume 30, pp. 353–362.
51. Brocca, L.; Melone, F.; Moramarco, T. Distributed rainfall-runoff modelling for flood frequency estimation and flood forecasting. *Hydrol. Processes* **2011**, *25*, 2801–2813. [CrossRef]
52. Mitchell, J.; Banasik, K.; Hirschi, M.; Cooke, R.; Kalita, P. There is not always surface runoff and sediment transport. In *Proceedings of the Soil Erosion Research for the 21st Century: Proceedings of the International Symposium, Honolulu, HI, USA, 3–5 January 2001*; pp. 575–578.

53. Bazzi, H.; Baghdadi, N.; El Hajj, M.; Zribi, M.; Belhouchette, H. A comparison of two soil moisture products S 2 MP and copernicus-SSM over southern France. *IEEE J. Sel. Top. Appl. Earth Obs. Remote Sens.* **2019**, *12*, 3366–3375. [CrossRef]
54. Rabiei, S.; Jalilvand, E.; Tajrishy, M. A Method to Estimate Surface Soil Moisture and Map the Irrigated Cropland Area Using Sentinel-1 and Sentinel-2 Data. *Sustainability* **2021**, *13*, 11355. [CrossRef]
55. Attarzadeh, R.; Amini, J.; Notarnicola, C.; Greifeneder, F. Synergetic use of Sentinel-1 and Sentinel-2 data for soil moisture mapping at plot scale. *Remote Sens.* **2021**, *10*, 1285. [CrossRef]